

Optics Letters

Enhanced super resolution using Fresnel incoherent correlation holography with structured illumination

YUVAL KASHTER,^{1,*} A. VIJAYAKUMAR,¹ YOKO MIYAMOTO,² AND JOSEPH ROSEN¹

¹Department of Electrical and Computer Engineering, Ben-Gurion University of the Negev, P.O. Box 653, Beer-Sheva 8410501, Israel

²Department of Engineering Science, The University of Electro-Communications, 1-5-1, Chofugaoka, Chofu, Tokyo 182-8585, Japan

*Corresponding author: kashter@bgu.ac.il

Received 13 January 2016; accepted 22 February 2016; posted 29 February 2016 (Doc. ID 257413); published 29 March 2016

The structured illumination (SI) technique has already been well established as a resolution enhancer in many studies and well demonstrated in many optical imaging systems during the past decade. The ability to use the SI in incoherent imaging systems was also introduced, especially in fluorescence microscopy. In this Letter, we propose and demonstrate a new approach to combine the SI technique with the recently innovated motionless incoherent holographic system, called Fresnel incoherent correlation holography (FINCH), in order to enhance the resolution beyond the limits achieved in regular imaging with SI. The results obtained by use of SI-FINCH were compared against regular imaging, regular FINCH and SI-imaging. © 2016 Optical Society of America

OCIS codes: (100.6640) Superresolution; (090.1995) Digital holography; (110.0110) Imaging systems; (110.0180) Microscopy; (090.1760) Computer holography; (050.5080) Phase shift.

<http://dx.doi.org/10.1364/OL.41.001558>

In 2000, Gustafsson proposed and demonstrated the idea of structured illumination (SI) microscopy [1]. The underlying idea of SI-imaging is the use of patterned light illumination in order to shift the spatial frequency spectrum of the observed object. By this shifting, high frequencies are transferred through the imager, instead of being cut off by the system's limited optical transfer function (OTF). Hence, the effective OTF of the system can be precisely expanded by the use of SI with different frequencies and orientations, while maintaining the same physical dimensions of the imager's aperture. Consequently, the SI technique has been used to improve the resolving power of the imaging systems without varying the illuminating wavelength or the physical aperture dimensions.

Imaging can be broadly classified into coherent and incoherent imaging. Coherent imaging systems suffer from numerous problems such as edge ringing, speckle noise, etc., and, hence, low cost, laser-less incoherent imaging systems are preferred for imaging [2] in most cases. The implementation of the SI technique in incoherent imaging systems has been demonstrated (e.g., Gustafsson *et al.* in his SI based microscopy with scrambled

laser light [1] and fluorescence light [3]). A comprehensive review about SI in optical microscopy is presented in Ref. [4]. Gao *et al.* have implemented the technique of SI in a coherent digital holographic microscope [5]. In this Letter, we introduce the concept of SI into the field of incoherent digital holography.

In 2007, a digital incoherent holographic system known as the Fresnel incoherent correlation holography (FINCH) was invented [6,7]. FINCH falls under the category of self-informative-reference holography, which violates the Lagrange invariant conditions of classical optical systems [8–10]. In general, the OTF width of regular incoherent imaging systems is twice as that of an equivalent coherent imaging system, but its frequency response decreases to zero with respect to the frequency magnitude, affecting the imaging resolution. In the case of FINCH [11] and other self-informative-reference hologram recorders [12], the width of the OTF can be the same as that of any incoherent imaging system, but, ideally, it has a uniform response along all frequencies up to the cut-off frequency. Due to its OTF profile, FINCH exhibits a higher resolving power by a factor of about 1.5 than a regular incoherent imaging system, with the same NA [11]. As a result, the SI implemented in FINCH has the potential to resolve objects beyond the limit of the SI implemented in regular incoherent imaging. Resolution enhancement in FINCH has already been demonstrated using synthetic aperture with Fresnel elements (SAFE) [13], and by designing an optimal SAFE setup [14]. However, unlike SI systems, the SAFE techniques have not been implemented in microscopy so far, since a way of constructing a synthetic aperture in FINCH equipped with a microscope objective has not been found yet.

In this Letter, we present the design, experimental investigation, and results of resolution enhancement using the dual lens FINCH [11,15] combined with the SI technique, called SI-FINCH.

The proposed SI-FINCH is presented in Fig. 1, where the additional part, represented by the dashed square, enables the implementation of the SI technique. A spatially incoherent light source is collimated by a refractive lens, L_1 , and is projected on a transmissive amplitude spatial light modulator (SLM), denoted as SLM_1 , on which four groups of periodic

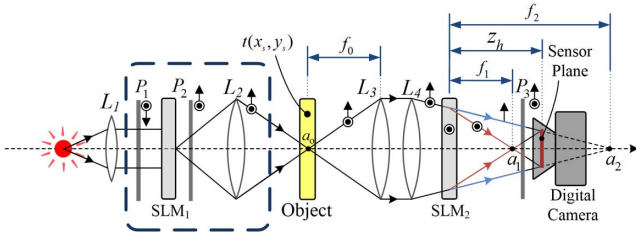


Fig. 1. Optical configuration of the SI-FINCH based on the dual lens FINCH.

functions with sinusoidal profiles along horizontal, vertical, and two diagonal orientations are displayed. The illuminated periodic patterns are imaged on an object by a lens, L_2 . In order to image the pattern displayed on SLM_1 onto the object plane with maximum contrast, it is required to position two linear polarizers mutually perpendicular to each other on either side of the SLM. Thus, two polarizers, P_1 and P_2 , are placed before and after SLM_1 , respectively, with polarization orientations orthogonal to one another. In accordance with the previous FINCH study [16], the maximal visibility of the interference pattern is achieved by orienting two polarizers, P_2 and P_3 , placed before and after the phase SLM (SLM_2 in Fig. 1) at 45° with respect to the SLM modulation axis. Consequently, the axes of P_1 , P_2 , and P_3 are all oriented at 45° with respect to the modulation axis of SLM_2 , in such a way that P_1 and P_2 are orthogonal to each other and P_2 and P_3 are parallel to each other. On SLM_2 , a pattern of a diffractive lens is displayed. The lens L_3 , with a focal length of f_0 , is used as a collimation lens and the lens L_4 implements the dual lens FINCH principle [11] by converting the plane wave into a spherical wave. Beyond SLM_2 , two spherical waves are created with perpendicular polarization orientations, with focal distances of f_1 and f_2 , respectively. The polarizer P_3 oriented at 45° allows the propagation of only the projections of the two spherical waves oriented with the same polarization of P_3 , and by that, the interference between the waves on the sensor plane (the hologram plane located at z_h from SLM_2) is enabled. The focal length of the diffractive lens (displayed on SLM_2) is determined in accordance with the following expression:

$$f_a = f_2 f_1 / (f_2 - f_1). \quad (1)$$

The four groups of gratings, imaged from SLM_1 on the object plane by L_2 , are given by equation (2) as follows:

$$\Psi_m(x_s, y_s; \Phi) = \frac{1}{2} \times \begin{cases} 1 + \cos(2\pi\nu x_s + \Phi), & m = 1 \\ 1 + \cos(2\pi\nu y_s + \Phi), & m = 2 \\ 1 + \cos(2\pi\nu(x_s + y_s)/\sqrt{2} + \Phi), & m = 3 \\ 1 + \cos(2\pi\nu(x_s - y_s)/\sqrt{2} + \Phi), & m = 4, \end{cases} \quad (2)$$

where $\Phi = 0, \pi/2, \pi$, and $3\pi/2$, represents the four phase shifts imposed on the gratings, ν is the spatial frequency of the gratings, and the transverse position at the object plane is represented by $\vec{r}_s = (x_s, y_s)$.

According to previous mathematical analyses of FINCH [6,11], the point spread function (PSF) of every object point can be described as

$$I(\vec{r}_0, \vec{r}_s; \theta) = \left(C_1 + C_2(\vec{r}_s) Q\left(-\frac{1}{z_r}\right) L\left(\frac{-\vec{r}_r}{z_r}\right) \exp(-i\theta) + C_2^*(\vec{r}_s) Q\left(\frac{1}{z_r}\right) L\left(\frac{\vec{r}_r}{z_r}\right) \exp(i\theta) \right) \times \text{circ}(r_r/R), \quad (3)$$

where $\vec{r}_0 = (x_0, y_0)$ is the location vector of the sensor plane, Q designates the quadratic phase function of the form $Q(b) = \exp[i\pi b \lambda^{-1}(x^2 + y^2)]$, λ is the central wavelength of the light source, L denotes the linear phase function of the form $L(\vec{s}) = \exp[i2\pi\lambda^{-1}(s_x x + s_y y)]$, C_1 is a real constant, and $C_2(\vec{r}_s)$ is a complex constant dependent on the location of the point source. The argument $\theta = 0, 2\pi/3$, and $4\pi/3$ are the phase shifting values employed to eliminate the twin image and the bias terms from the final hologram as specified in Ref. [6]. The limiting aperture function is a circular function defined by

$$\text{circ}\left(\frac{r_r}{R}\right) \equiv \begin{cases} 1 & x^2 + y^2 \leq R^2 \\ 0 & \text{otherwise} \end{cases},$$

where R represents the radius of the aperture. The vector $\vec{r}_r = (x_r, y_r)$ is the transversal location of the reconstructed image point given by $\vec{r}_r = (x_r, y_r) = (x_s z_h / f_0, y_s z_h / f_0)$. The parameter z_r is the reconstruction distance from the hologram plane (sensor plane) given by

$$z_r = \pm \frac{(z_h - f_1)(f_2 - z_h)}{f_2 - f_1}, \quad (4)$$

where z_h is calculated [11], in order to achieve perfect overlap between the two interfering spherical waves, as follows:

$$z_h = \frac{2f_1 f_2}{f_1 + f_2}. \quad (5)$$

The \pm in Eq. (4) indicates that there are two possible reconstruction distances, although only one of them is chosen. According to the PSF given by Eq. (3), the mathematical expression representing a complete Fresnel hologram of a general object, with an intensity distribution of $I_s(x_s, y_s)$, illuminated by a spatially incoherent and quasi-monochromatic source, through any m th periodic grating $\Psi_m(x_s, y_s; \Phi)$, is given as

$$H_m(\vec{r}_0; \theta; \Phi) = [I_s(\vec{r}_s) \Psi_m(\vec{r}_s; \Phi)] * I(\vec{r}_0; \vec{r}_s; \theta), \quad (6)$$

where the asterisk denotes 2D convolution.

Eventually, three holograms were recorded with three phase shift angles θ of SLM_2 for each of the four phase shift angles Φ of SLM_1 resulting in a total of 12 holograms. This procedure was repeated along the four m orientations according to Eq. (2) resulting in a total of 48 exposures. Following early FINCH studies [6,7], for every grating orientation corresponding to different values of m and for every phase shift Φ in SLM_1 , the superposition of the three recorded holograms with the three above mentioned θ angles is performed as follows:

$$\begin{aligned}
u_{H_m}(\bar{r}_0; \Phi) = & H_m(\bar{r}_0; \theta = 0; \Phi)[\exp(-i4\pi/3) - \exp(-i2\pi/3)] \\
& + H_m(\bar{r}_0; \theta = 2\pi/3; \Phi)[1 - \exp(-i4\pi/3)] \\
& + H_m(\bar{r}_0; \theta = 4\pi/3; \Phi)[\exp(-i2\pi/3) - 1]. \quad (7)
\end{aligned}$$

The SI duplicates the object's spatial spectrum and distributes the duplications among various diffraction orders. In order to eliminate all the diffraction orders except the first order, a process with four phase shifts is performed with the gratings of the SI. The reason for using four Φ phases instead of three is because four phases also guarantees the elimination of orders higher than the first order, which might appear in the case that the SI grating does not have a perfect sinusoidal profile. For any m th orientation, the four complex holograms were superposed according to the following expression:

$$\begin{aligned}
u_m(\bar{r}_0) = & u_{H_m}(\bar{r}_0; \Phi_1) - u_{H_m}(\bar{r}_0; \Phi_3) \\
& - [u_{H_m}(\bar{r}_0; \Phi_2) - u_{H_m}(\bar{r}_0; \Phi_4)]i. \quad (8)
\end{aligned}$$

Next, four reconstructed images, represented by S_m , were produced by applying the Fresnel back propagation operation [6–11]. Recall that each image originated from the first diffraction order is located along a different m axis. Each image should be compensated by a corresponding linear phase function before the four images are summed up to obtain the final image. The final image is as follows:

$$\begin{aligned}
S_{\text{total}}(\bar{r}_r) = & S_1(\bar{r}_r) \exp(-i2\pi\nu_r x_r) \\
& + S_2(\bar{r}_r) \exp(-i2\pi\nu_r y_r) \\
& + S_3(\bar{r}_r) \exp\left(-i2\pi\nu_r(x_r + y_r)/\sqrt{2}\right) \\
& + S_4(\bar{r}_r) \exp\left(-i2\pi\nu_r(x_r - y_r)/\sqrt{2}\right), \quad (9)
\end{aligned}$$

where the frequency $\nu_r = \nu/M_T$; M_T represents the transverse magnification and it equals z_b/f_0 .

The SI-FINCH system was demonstrated by an experimental procedure that was carried out in accordance with the setup shown in Fig. 1. In order to demonstrate the resolution capabilities of the dual lens SI-FINCH and its advantages, we compared its results with those of a regular incoherent imaging system under identical optical conditions and with a FINCH system without SI. Moreover, in order to analyze the system response to different SI frequencies, we also compared the corresponding results of SI patterns with two different spatial frequencies. Two periodic patterns (24 and 48 lp/mm) with sinusoidal profiles were displayed on SLM₁ (Holoeye LC2012, 1024 × 768, 36 μm pixel pitch), which was illuminated by a LED (Thorlabs LED 631E, 4 mW, λ = 635 nm, Δλ = 10 nm). The SI illuminated a section (Groups 6 and 7) of the USAF chart mounted at the object plane. In order to implement the dual lens FINCH, a phase-only SLM (Holoeye PLUTO, 1920 × 1080 pixels, 8 μm pixel pitch) was used as SLM₂. A diffractive lens with a focal length $f_{\text{SLM}} = 640$ mm was displayed on the SLM. The size of the diffractive lens was limited by a circular aperture with a radius of 540 pixels (4.32 mm). Additionally, the lenses L_3 and L_4 were chosen to be glass bi-convex spherical lenses with an aperture diameter of 50.8 mm, where their focal lengths are $f_0 = 200$ mm and $f_{L_4} = 1000$ mm, respectively. Three polarizers P_1 , P_2 , and P_3 (rotated by 45°) were placed

according to Fig. 1. As a result, two converging spherical waves, with the focal distances $f_1 = 381.6$ mm and $f_2 = 945$ mm, were interfered on a sensor camera (GigE vision GT Prosilica, 2750 × 2200 pixels, 4.54 μm pixel pitch), which was placed in a distance of $z_b = 543.6$ mm [according to Eq. (5)].

To implement the above mentioned conventional imaging system with the same setup, shown in Fig. 2, the focal distance of the diffractive lens displayed on SLM₂ was modified to $1280 \approx 945 \times 543.6 / (945 - 543.6)$ mm. For the experiment of the SI-imaging, 16 images were grabbed, corresponding to four different values of Φ and for each of the four different grating orientations. In order to have a genuine comparison between the SI-FINCH and SI-imaging, the periodic functions with the same frequencies were displayed on SLM₁. In addition, both of the SI-systems (conventional and FINCH) were compared to regular imaging and FINCH systems in which the objects were illuminated by uniform light without any SI [Figs. 3(a) and 3(b)]. This uniform illumination was implemented by displaying a uniform matrix of the values of one on SLM₁.

For an object located at the front focal plane of a collimation lens with a focal length of 200 mm illuminated by a central wavelength of $\lambda = 635$ nm and observed by a circular aperture with a radius of 4.32 mm, the minimal transversal distance that can be resolved, according to the Rayleigh criterion, is $1.22 \cdot 0.635 \cdot 200 / (2 \cdot 4.32) \approx 17.9$ μm (i.e., Maximum frequency of 56 lp/mm). Therefore, the finest section that can be resolved in the resolution chart is the element 5 of group 5 (50.8 lp/mm). Figures 3(a) and 3(b) demonstrate that the resolving power of FINCH is greater than that of an equivalent incoherent imaging system (as already proved and demonstrated in previous FINCH studies [9,11]). Following previous SI-imaging studies [4], the effective cut-off frequency is the sum of the inherent cut-off frequency and the frequency of the SI grating. Based on an aperture radius of 4.32 mm, a focal length of 200 mm, and $\lambda = 635$ nm, the inherent cut-off frequency is $2 \cdot 4.32 / (0.635 \cdot 0.2) \approx 68$ lp/mm. Therefore, implementing the SI technique with 24 and 48 lp/mm illumination gratings in a conventional imaging system creates corresponding effective cut-off frequencies of 92 and 116 lp/mm, respectively. In other words, theoretically for the two SI frequencies, the finest sections that are supposed to be perceived at the resolution chart are element 4 in group 6 (90.5 lp/mm) and element 6 in group 6 (114 lp/mm), respectively.

In order to precisely define the resolution limits of regular imaging, regular FINCH, SI-Imaging, and SI-FINCH, the average of the intensity distribution of both USAF chart gratings in each finest element, that can still be resolved according to the Rayleigh criterion, was calculated (see graphs in Fig. 3).

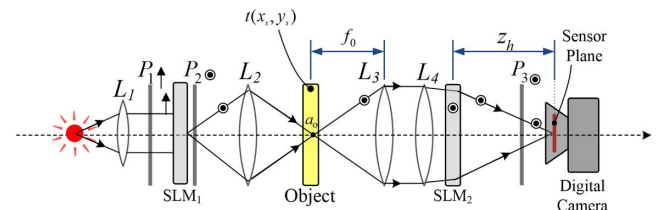


Fig. 2. Optical configuration of the SI-imaging based on the same optical arrangement as that of the SI-FINCH.

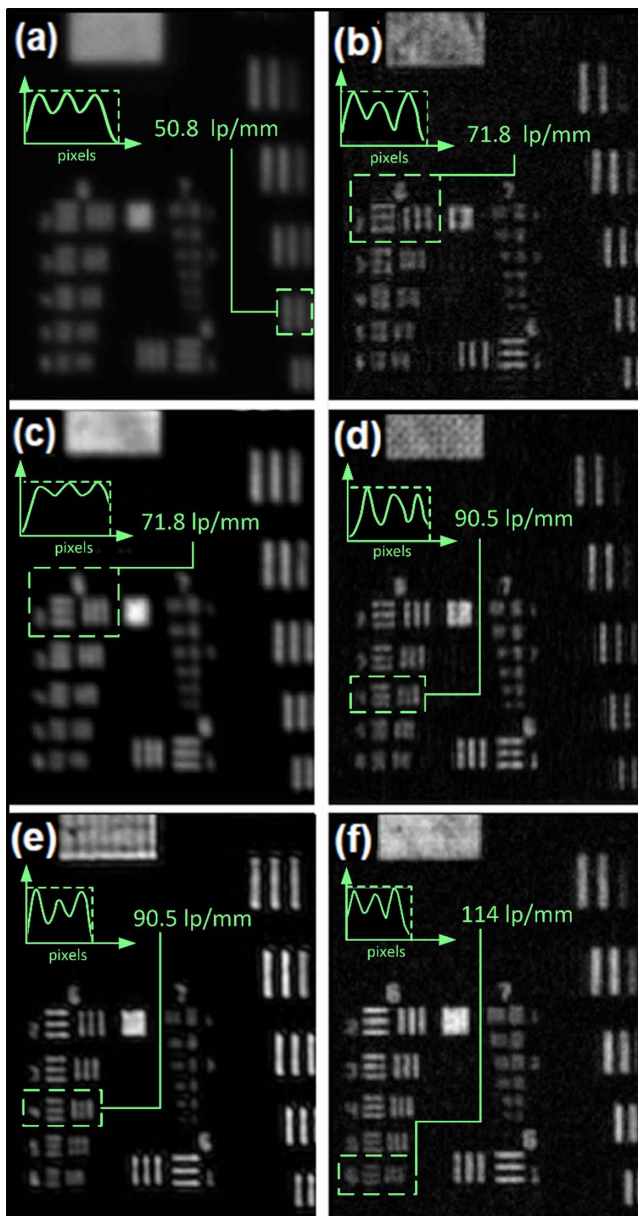


Fig. 3. Experimental results obtained by recording a section (groups 6 and 7) of the USAF target by the four systems mentioned in the text: (a) the image obtained by the conventional imaging system shown in Fig. 2 with uniform illumination; (b) the reconstructed image corresponding to the dual lens FINCH system shown in Fig. 1 with uniform illumination; (c) the image obtained by the SI-imaging system with a SI grating of 24 lp/mm; (d) the image obtained by the SI-FINCH system with a SI grating of 24 lp/mm; (e) the image obtained by the SI-imaging system with a SI grating of 48 lp/mm; (f) the image obtained by the SI-FINCH system with a SI grating of 48 lp/mm. The dashed areas represent the finest elements that can be resolved according to the Rayleigh criterion; the 1D graphs represent the average normalized intensity of both gratings in each finest element.

To satisfy the Rayleigh criterion, it is necessary that the minimal dip should be at least 26.3% of the maxima.

According to Figs. 3(c) and 3(e), one can realize that the involvement of the SI technique, indeed, improves the resolution capabilities of the incoherent imaging system [compared to

Fig. 3(a)]. However, the finest details that can be resolved by the SI-imager is element 2 in group 6 (71.8 lp/mm) in Fig. 3(c) and element 4 in group 6 (90.5 lp/mm) in Fig. 3(e). These results support the theoretical observation that the OTFs of incoherent imaging systems monotonically decrease to zero with the increase in frequencies. Thus, these systems of SI-imaging do not fully exploit the increase of the effective bandwidth. Figures 3(d) and 3(f) demonstrate the uniform response of the SI-FINCH OTFs for all frequencies; the three lines along the vertical and horizontal orientations in element 4 of group 6 (90.5 lp/mm), and in element 6 of group 6 (114 lp/mm) can be clearly perceived in Figs. 3(d) and 3(f), respectively.

In conclusion, we have proposed and demonstrated a new procedure for integrating the SI technique into the FINCH technology in order to improve the imaging resolution beyond the limit achievable using SI-imaging. In the optical configuration employed, SI-imaging was found to resolve lines separated by 14 and 11 μm , while SI-FINCH was able to resolve lines separated as small as 11 and 8.8 μm , corresponding to SI frequencies 24 and 48 lp/mm, respectively. These results demonstrate a resolution enhancement factor of about 1.3 of the SI-FINCH over the SI-imaging. Note that although the spatial bandwidth has been extended by factors of $1.35 \approx (68 + 24)/68$ and $1.7 \approx (68 + 48)/68$, the overall resolution enhancement factors of SI-FINCH over the regular imager are $1.78 \approx 90.5/50.8$ and $2.24 \approx 114/50.8$ corresponding to SI frequencies 24 and 48 lp/mm, respectively. We believe that, introducing SI into FINCH or other self-informative-reference hologram recorders [12,17] can substantially enhance the resolving power of many 3D microscopes.

Funding. The Israel Ministry of Science, Technology, and Space; Israel Science Foundation (ISF) (439/12); University of Electro-Communications (UEC), Japan.

Acknowledgment. The authors thank Dr. Roy Kelner for invaluable discussions.

REFERENCES

1. M. G. L. Gustafsson, *J. Microsc.* **198**, 82 (2000).
2. P. S. Conside, *J. Opt. Soc. Am.* **56**, 1001 (1966).
3. M. G. L. Gustafsson, L. Shao, P. M. Carlton, C. J. R. Wang, I. N. Golubovskaya, W. Z. Cande, D. A. Agard, and J. W. Sedat, *Biophys. J.* **94**, 4957 (2008).
4. M. Saxena, G. Eluru, and S. S. Gorthi, *Adv. Opt. Photon.* **7**, 241 (2015).
5. P. Gao, G. Pedrini, and W. Osten, *Proc. SPIE* **8788**, 878809 (2013).
6. J. Rosen and G. Brooker, *Opt. Lett.* **32**, 912 (2007).
7. J. Rosen and G. Brooker, *Opt. Express* **15**, 2244 (2007).
8. P. Bouchal, J. Kapitán, R. Chmelík, and Z. Bouchal, *Opt. Express* **19**, 15603 (2011).
9. J. Rosen and R. Kelner, *Opt. Express* **22**, 29048 (2014).
10. X. Lai, S. Xiao, Y. Guo, X. Lv, and S. Zeng, *Opt. Express* **23**, 31408 (2015).
11. J. Rosen, N. Siegel, and G. Brooker, *Opt. Express* **19**, 26249 (2011).
12. R. Kelner, J. Rosen, and G. Brooker, *Opt. Express* **21**, 20131 (2013).
13. B. Katz and J. Rosen, *Opt. Express* **19**, 4924 (2011).
14. Y. Kashter and J. Rosen, *Opt. Express* **22**, 20551 (2014).
15. B. Katz, J. Rosen, R. Kelner, and G. Brooker, *Opt. Express* **20**, 9109 (2012).
16. G. Brooker, N. Siegel, V. Wang, and J. Rosen, *Opt. Express* **19**, 5047 (2011).
17. C. Jang, J. Kim, D. C. Clark, B. Lee, and M. K. Kim, *J. Biomed. Opt.* **20**, 111204 (2015).